buildings

MDPI

Article

Uncertainty Assessment of Mean Radiant Temperature Estimation for Indoor Thermal Comfort Based on Clustering Analysis of Reduced-Input Surfaces

Eunho Kang [1], Ruda Lee [1], Jongho Yoon [1], Heejin Cho [2] and Dongsu Kim [1,*]

[1] Department of Architectural Engineering, Hanbat National University, Daejeon 34158, Republic of Korea
[2] Department of Mechanical Engineering, Mississippi State University, 210 Carpenter Engineering Building, Starkville, MS 39762, USA
* Correspondence: dongsu.kim@hanbat.ac.kr; Tel.: +82-042-821-1122

Abstract: Mean radiant temperature (MRT) is important for indoor thermal comfort determination. Several good ways to practically obtain accurate MRT include measuring all indoor surface temperatures for MRT calculation or using a black globe thermometer. Still, it can be hard to apply in practice because using such experimental measurements increases the efforts of data management times and acquisition costs. In this regard, there is a practical advantage in reducing the number of measured surfaces by grouping similar surfaces rather than measuring all indoor surface temperatures individually to obtain MRT. However, since even those similar surfaces are not the same, it can lead to erroneous MRT estimation, which needs to be investigated. This study analyzes the uncertainty of MRT estimates by categorizing the surfaces with similar temperature behaviors to examine the risk of such inaccuracy. In this study, the input data required for the MRT calculation are generated using a measurement data-based simulation model, and the uncertainty of the MRT is quantified using the Monte Carlo method. As a result of the study, it is observed that excluding surfaces with similar temperatures for MRT estimation does not significantly affect the uncertainty. When the appropriate number of input surfaces is satisfied, its MRT shows a difference of less than 1% compared to the results calculated with all surfaces.

Keywords: mean radiant temperature; plane radiant temperature; uncertainty analysis; thermal comfort

check for updates

Citation: Kang, E.; Lee, R.; Yoon, J.; Cho, H.; Kim, D. Uncertainty Assessment of Mean Radiant Temperature Estimation for Indoor Thermal Comfort Based on Clustering Analysis of Reduced-Input Surfaces. *Buildings* **2023**, *13*, 342. https://doi.org/10.3390/buildings13020342

Academic Editors: Paulo Santos and Mark Bomberg

Received: 11 January 2023
Revised: 18 January 2023
Accepted: 19 January 2023
Published: 26 January 2023

Copyright: © 2023 by the authors. Licensee MDPI, Basel, Switzerland. This article is an open access article distributed under the terms and conditions of the Creative Commons Attribution (CC BY) license (https://creativecommons.org/licenses/by/4.0/).

1. Introduction

Indoor environment quality can be affected by many related factors, such as heat, acoustic and visual conditions, and indoor air quality. In particular, indoor thermal comfort is a very important factor related to the health of occupants [1]. According to the definition of ASHRAE 55 [2], thermal comfort is achieved by maintaining a thermal balance between the human body and the surrounding environment, so it is determined by the physical parameters of the surrounding environment and the occupant's condition.

Therefore, since various variables determine thermal comfort, indicators such as the predicted mean vote (PMV) are widely used to represent it. PMV represents thermal comfort using two parameters (metabolism, clothing) related to occupant's condition and four parameters (air temperature, mean radiant temperature, air velocity, and humidity) associated with the indoor environment. PMV is widely used to indicate indoor thermal comfort. PMV represents thermal comfort by considering heat transfer between the human body and the surrounding environment using the occupant's state and indoor physical variables. This indicator was developed through experimental research by Fanger [3], and it is introduced as an indicator of thermal comfort in ISO 7730 [4] and ASHRAE 55 [2]. Because estimating all input parameters for PMV calculation requires much effort and resources in a field [5], it is relatively hard to obtain accurate PMV estimates practically.

In particular, the mean radiation temperature (MRT), one of the parameters required for PMV calculation, is a particular variable and a physical parameter that greatly affects PMV significantly. MRT is defined as the surface temperature of a blackbody that radiates from its surrounding surface a radiative heat flux equal to the radiative heat flux incident on that point [4]. Therefore, in a room surrounded by warm surfaces, which is an environment with a high MRT, occupants can feel the warmth even when the ambient air temperature is low. Similarly, if there are cold walls or windows around the occupant, the occupant may feel cold even if the air temperature is within comfortable ranges [6,7]. Because the calculation requires a professional measuring instrument to obtain physical and personal variables [8,9], MRT is often assumed to be simplified, which may increase uncertainty about indoor thermal comfort [10].

Many studies have shown that inaccurate MRT observations can be a source of PMV uncertainty. Ekici (2016) [11] reported that the ambient air temperature and MRT among the input variables of PMV have the most direct influence on the uncertainty of thermal comfort. Chaudhuri et al. (2016) [12] also showed that assumptions considering MRT equal to ambient air temperature could cause large errors in thermal comfort estimation, which means that error propagation of MRT can result in inaccurate indoor comfort controls. Accordingly, although measuring MRT is difficult in an accurate manner, the procedure for observing MRT needs to be considered for PMV calculation because it significantly affects thermal comfort behaviors [13–15]. ISO 7726, an international standard, introduces the method of using the globe temperature and the angle factor method using the ambient surface temperature as a method of observing the mean radiant temperature [13,16].

Measurement of MRT with the globe temperature is a commonly used method [17] because the price of the measuring instrument is relatively low and easy to use. This method can calculate the MRT using three parameters: the globe temperature, air temperature, and air velocity around the globe thermometer. However, the response time (20–30 min) is high, and it may cause inconvenience to occupant activities because it must be installed in all locations where measurement is required [9,15].

Since the angle factor method calculates the MRT by taking the surface temperature and angle factor between the human body and the surrounding surfaces as inputs, the measuring sensor of surface temperatures, such as a contact thermometer or an infrared thermometer, is used. Contact thermometers are inexpensive and relatively handy for measuring temperature. However, since the reliability of the measured value may be reduced due to contact resistance, steady management is required. In the case of an infrared thermometer, there is an advantage in usability because it can measure remotely. The measurement value is greatly affected by the physical properties of the surface and the measurement environment. Therefore, the target surface's historical emissivity and reflectance values are required. Additionally, the user's expertise is necessary to correct the error caused by the measurement environment [18,19].

In the case of the measurement of MRT with a global thermometer, the accuracy is high, but since it provides only the MRT for the measurement location, there is a disadvantage that it may cause inconvenience to occupants' activities due to the installation of the measuring instrument. On the other hand, in the case of the angle factor method, since the physical relationship of the surrounding surfaces is used, it is possible to calculate the MRT of not only a single point but also all points in the room. It is also possible to evaluate the radiation asymmetry using the plane radiant temperature. It has been reported that the MRT derived by the calculation method using the surface temperature is reliable with an error of about 1 °C [8].

Data observation and management costs may increase if the angle factor method is used because most of the surrounding surface temperature must be measured. However, when calculating the room's surface temperature, since the surfaces exist in the same space, a similar pattern is shown except for the surface strongly influenced by external conditions or heating equipment. Therefore, if the MRT is derived by representing similar surfaces with one surface after grouping similar surfaces in advance, the number of surface

temperatures, which are input variables for calculation, is reduced, so there may be practical advantages such as data measurement cost reduction.

There have been various previous studies to reduce the resources required for MRT calculation. Vorre et al. (2015) [20] geometrically simplified the human body shape to reduce the amount of computation necessary for MRT calculation. They compared it with the results of complex methods such as ray tracing. Dogan et al. (2021) [21] predicted outdoor MRT with an accuracy of about ±2 °C by clustering surrounding surfaces. However, few studies have simplified indoor MRT prediction methods by grouping indoor surfaces. In addition, no study has explored uncertainty analysis due to the simplification method of MRT calculation. Even though indoor surfaces are on similar boundary conditions, they are not the same, so if some surfaces are considered equally and the average radiant temperature is calculated, an error will inevitably occur. When the error for MRT observation becomes large, thermal comfort may be incorrectly evaluated, so it is necessary to investigate the uncertainty in advance for reliable indoor MRT observation [22,23]. In this study, to quantitatively analyze the reliability of the MRT calculated according to the grouping of similar surface temperatures, the uncertainty of MRT due to the reduction of surface temperature input is investigated through a case study.

2. Methodology

This study investigates the uncertainty of indoor MRT derived according to the indoor surface temperature grouping for a specific case. This study also analyzes the effect of the uncertainty of indoor thermal comfort. The input data for the MRT calculation are generated through a simulation model, and the Monte Carlo method is used to investigate the uncertainty. The overall research flow proceeds, as shown in Figure 1.

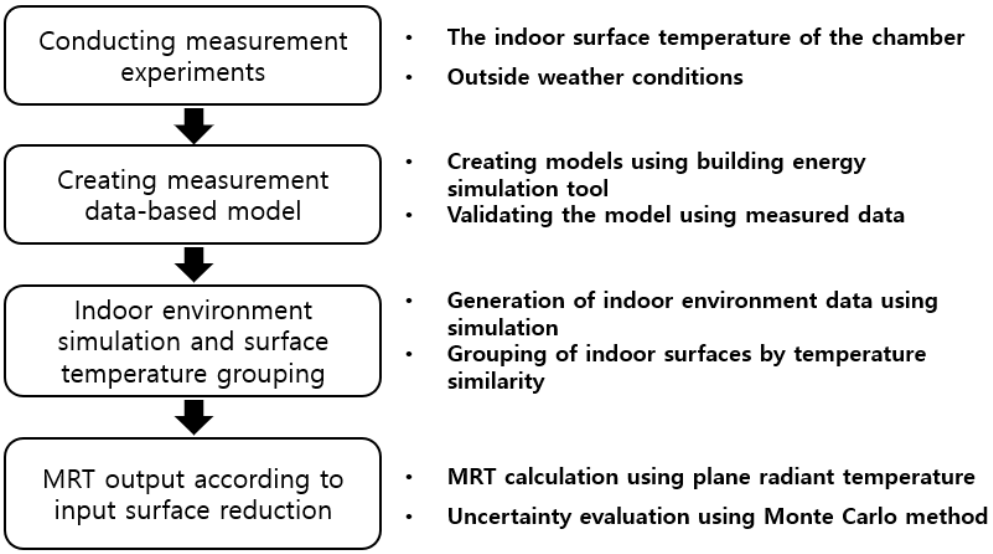


Figure 1. Flowchart of the research.

In steps 1 through 2, measurement experiments are conducted for simulation modeling for data generation. For the measurement data-based modeling, the chamber, in which the surface temperature measurement experiment is performed, is modeled using the building energy simulation program. The model is then validated by comparing the measured data with the model's output data. After the model validation, the second step is carried out. In step 3, as a data generation step, simulated results for MRT calculation are used as outputs, and then grouping is performed for surface temperatures. The main output variables are the indoor surface temperatures and the solar radiation transmitted into the room, simulated under the input conditions of a typical meteorological year. Then, clustering analysis is performed on the simulated surface temperature data to categorize the surfaces, including similar temperature behaviors. The final step is to calculate the MRT according

to the input surface temperature reduction and examine the uncertainty of the MRT. The MRT is calculated using the simulation outputs of the preceding steps, and the Monte Carlo method is used because uncertainty must also be taken into account. The Monte Carlo method is a technique used for estimating results, such as uncertainty values. Since it proceeds with sufficiently many iterations with input values randomly extracted from a set of input variables, almost all possible consequences can be derived. At this time, the variable input set is the grouped surface temperature, which is randomly selected from the group. The extracted surface temperature is an input to the MRT calculation by replacing the remaining surfaces in the group. After sufficiently repeating the trial, the results of all trials are aggregated to calculate the uncertainty and statistical indicators.

3. Models and Generation Datasets

3.1. Experimental Setup for Model Validation

The experiment to measure the indoor surface temperature was conducted for 8 days from May 4 to May 12 in a test facility located at Hanbat National University (Republic of Korea, Daejeon, latitude: 36.35, longitude: 127.30). Figure 2 shows a photograph and plan view of the test facility where the measurement experiment is conducted. The interior size of the test facility is 5.5 m × 2.4 m × 2.3 m (length × width × height), and a window (2.0 m × 1.0 m) is located on the south wall at 0.8 m from the floor. The south and roof surfaces are exposed to the outside air, and the remaining surfaces are in contact with the adjacent zone. The roof has a 5-degree slope. The facility envelope is composed of SIP (Structural Insulated Panels) with a thickness of 220 mm, and the thermal transmittance is 0.17 W/m^{2}K. The window on the south side is a fixed window made of triple glazing (6 mm Clear, 6 mm LowE, 6 mm LowE) and the thermal transmittance is 1.44 W/m^{2}K.

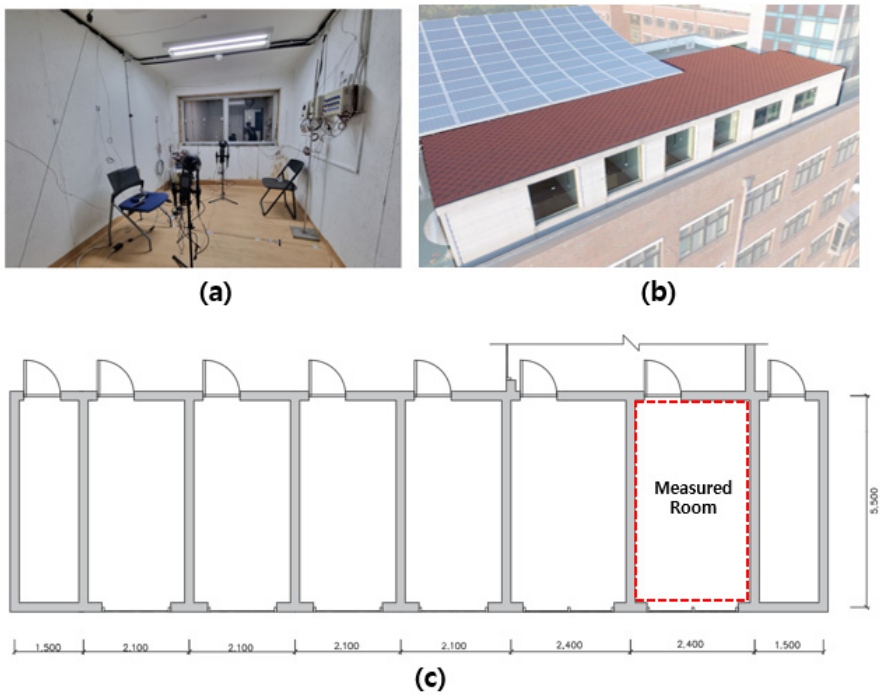


Figure 2. (**a**) Interior space of the chamber; (**b**) exterior view of the chamber; and (**c**) floor plan of the chamber.

To minimize heat transfer with the adjacent zone, the internal wall of the test chamber has the same insulation (220 mm, SIP) as the outer wall. The indoor surface temperature is measured using a thermocouple wire attached to each surface center point. The area-weighted average temperature of the frame, glass, and edge determines the window surface temperature. The temperature of the remaining surface is calculated by averaging the temperatures measured at three points in the center of each surface, and the average

surface temperature of each surface is assumed to be constant over the entire area of each surface. The measurement data was logged at 10 min intervals.

External meteorological data (e.g., external temperature and global horizontal irradiance) is also measured with 10 min of time-step. The outside temperature varied from 8.9 °C to 30.5 °C, the global horizontal irradiance was up to 1011 W/m^2, and the outside weather was mostly sunny during the experimental period. During the measurement period, the indoor thermal condition of the chamber was kept without the heating and cooling controls. As a result of the measurement, the indoor air temperature ranged from a minimum of 21.1 °C to a maximum of 28.6 °C due to the change in outdoor temperature and the influence of solar radiation, and the average daily temperature difference was 4.2 °C. In the case of indoor surface temperature, the average daily temperature difference of opaque surfaces such as walls and floors was 3.3 °C, but the average daily temperature difference between windows and doors was 7.1 °C, showing a relatively large range of changes. Figure 3 is a graph showing the measured indoor surface temperature and external weather conditions. The measuring instruments used in the measurement experiment are shown in Table 1.

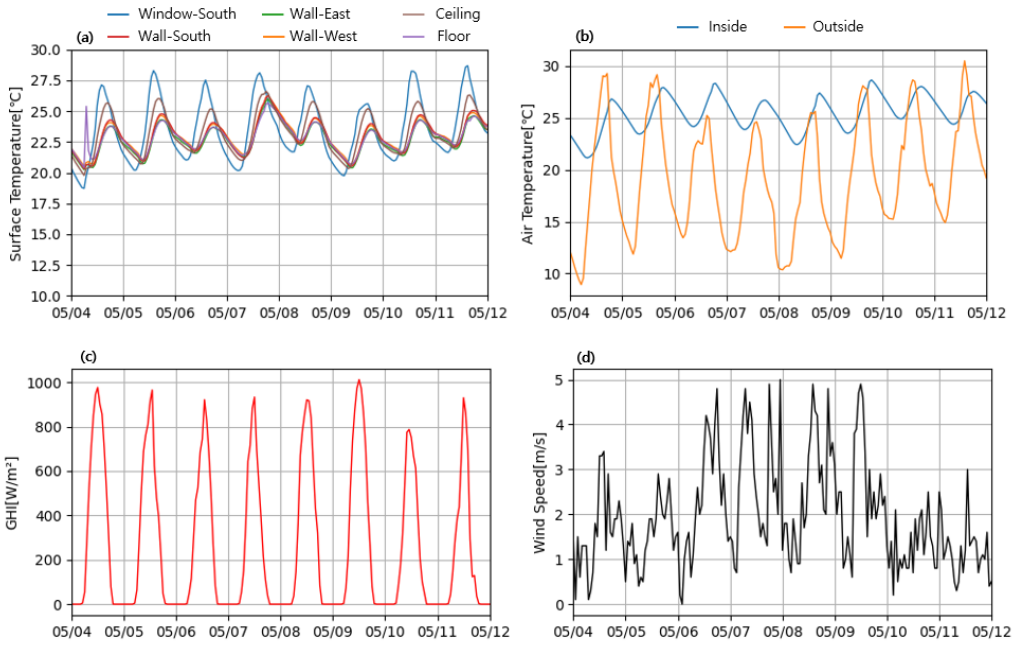


Figure 3. (**a**) Measured inside surface temperature; (**b**) measured internal and external air temperatures; (**c**) measured GHI (global horizontal irradiance); and (**d**) measured wind speed.

Table 1. Measurement equipment specifications used in the measurement experiment.

Variable	Instrument	Measuring Range	Accuracy
Dry Bulb Temperature	Thermocouple (T type)	−250 °C to 350 °C	±1.0 °C
Wind velocity	Hot Wire Anemometer	0 to 25 m/s	±5.0%
Global Solar Radiation	Pyranometer	0 to 2000 W/m^2	±15 W/m^2
Surface Temperature	Thermocouple (T type)	−250 °C to 350 °C	±1.0 °C

A simulation model of the test chamber is developed based on the geometry information from the experiment facility. The simulation model is created using the EnergyPlus [24] program, and its validity is checked by simulating the internal surface temperature under the same weather conditions as the measurement experiment. At this time, direct and diffuse components of solar radiation input to the simulation were determined using the Perez model [25], and parameter identification was performed using MCMC sampling to

improve data simulation accuracy [26]. The simulated chamber internal surface temperature and R2 of the measured data showed good similarity to 0.8 or more. Figure 4 is a graph comparing simulation results and measured data for surface temperature.

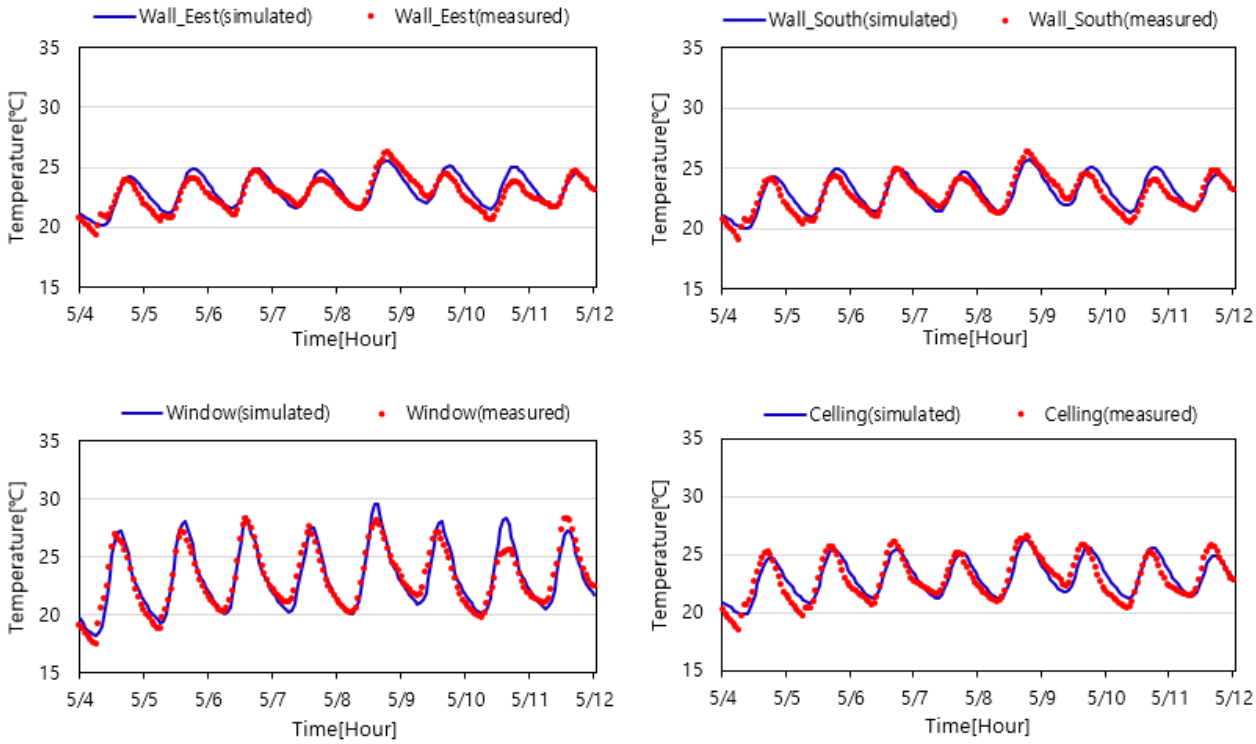


Figure 4. Comparison of measured and simulated surface temperature.

3.2. Generation of the Input Dataset

Input data required for MRT calculation is generated through the simulation model. The selected representative month of the typical meteorological year (TMY) is an input as the meteorological condition of the simulation. The TMY used for this analysis is the standard meteorological data of Daejeon, located in South Korea. The data is IWEC2 type TMY provided by ASHRAE [27]. The month with the lowest outdoor temperature of the TMY is in January, and the month with the highest is in August. In addition, the relative humidity in summer is higher than in other seasons. Accordingly, input data were generated in winter (January) and summer (August) weather conditions. The simulation period was 2 weeks from the 1st to the 14th of each month, and all result values were output at every 1-h step. Assuming that the room is controlled at a constant air temperature, the set temperature for cooling and heating is set at 25 °C for the entire simulation period.

Figures 5 and 6 show the simulation results under the set weather conditions. Figure 5 shows the indoor surface temperature, and Figure 6 shows the direct and diffusion components of irradiance transmitted into the room. The window's surface temperature clearly indicates a large difference compared to other surfaces. Especially in January, it shows a big difference under the influence of irradiance and low outside temperature. The surface temperature of the ceiling in August is higher than that of other surfaces except for windows due to the influence of irradiance during the day. In the case of irradiance transmitted indoors, the diffuse irradiance transmitted indoors was slightly higher in August than in January. In contrast, the direct irradiance transferred indoors was much higher in January than in August due to the influence of the solar's incident angle.

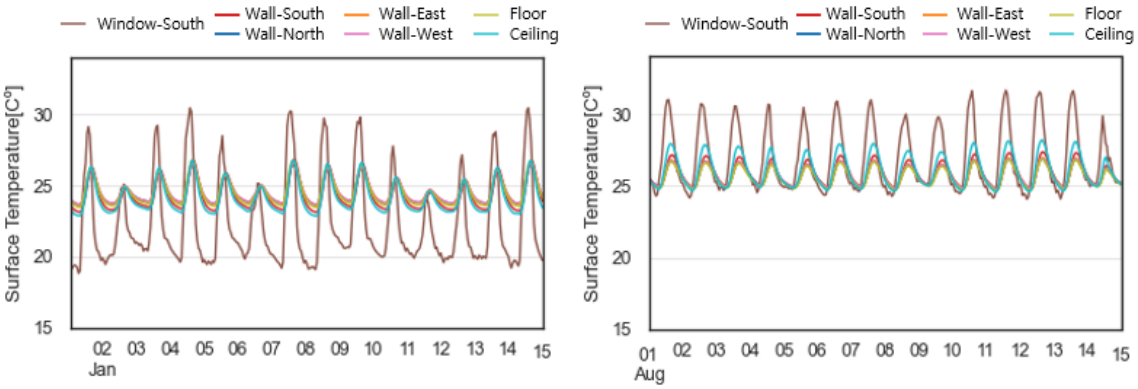


Figure 5. Simulation results: Indoor surface temperature: Winter (**left**), summer (**right**).

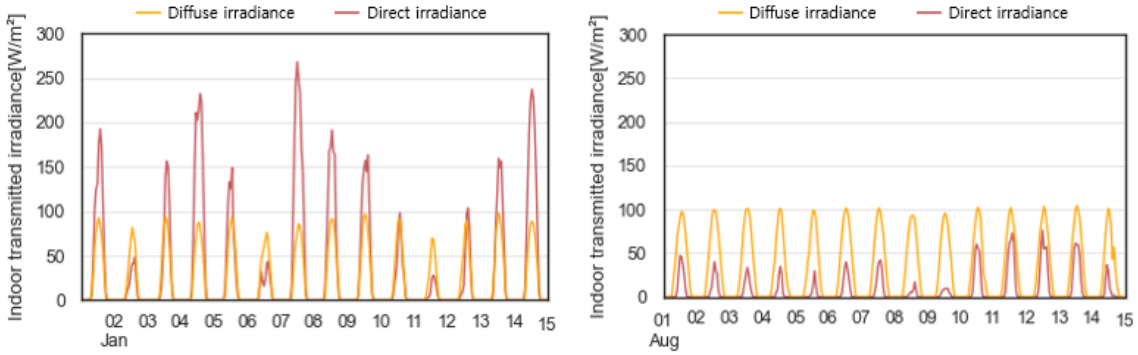


Figure 6. Simulation results: Indoor transmitted irradiance: winter (**left**), summer (**right**).

3.3. Grouping Indoor Surfaces Using Clustering

Clustering analysis is performed on the indoor surface temperature data to group surfaces exhibiting similar temperatures. Clustering is an unsupervised method that defines the similarity between data and clusters each data based on the similarity. Since MRT depends on the indoor conditions at the time, clustering is performed by calculating the Euclidean distance between data observed simultaneously. The k-mean algorithm was used as the cluster analysis algorithm to perform this analysis.

K-means was first proposed by M. Queen (1967) [28] as a clustering method that groups the given data into k number of clusters. The K-means algorithm classifies data based on the assumption that similar data are distributed around the centroid of each cluster. When the number (k) of clusters set by the user is given, a grouping of similar data is performed by continuously updating the centroid so that the distance between each data and the centroid of the cluster is minimized. K-mean clustering was performed according to the procedure below and was performed using Scikit-learn, a Python open-source library [29].

- Step (1) Randomly select the initial centroid of each cluster;
- Step (2) Calculate the similarity between the centroid and each data using Euclidean distance, and assign the data to the nearest cluster;
- Step (3) Update a new centroid for each cluster using the expectation-maximization algorithm;
- Step (4) If the selected center value satisfies the convergence condition, the center point update is stopped, and the finally calculated center value is adopted. If the convergence condition is not met, repeat steps 1–3.

Since clustering results may vary depending on randomly set central values, the expected results were used after performing clustering 30 times. As all 7 surfaces were classified into 6 groups from 2 groups, 5 types of clustering were performed, and the surface temperature for each time was used as the property for grouping the surfaces. The results of clustering are shown in the following Table 2.

Table 2. Clustering results for interior surfaces.

Count of Cluster		2	3	4	5	6
Window	South	2	2	2	2	2
Exterior Wall	South	1	3	4	4	4
Interior Wall	North	1	1	1	1	6
	West	1	1	1	1	1
	East	1	1	1	1	1
Floor		1	1	1	5	5
Ceiling		1	3	3	3	3

As a result of the clustering, when the surfaces are classified into two groups, the first group includes only the window surface, and the second group has all other surfaces. Since the window surface is most affected by the outside air, it is clearly differentiated from different surfaces. When the surfaces are classified into three groups, the surfaces in contact with the outside are organized into a new group. The surfaces classified into this group are the ceiling surface and the south wall surface. Then, as the number of clusters increases, a group, including a single surface, is created.

4. Calculation Method of Output

This section describes the mean radiant temperature and the PMV calculation procedure. To calculate these, the procedure presented in ISO7726 is mainly referred to, and since MRT may be affected by solar radiation transmitted through windows, the calculation method is modified by considering these effects [30]. In addition, these indicators are calculated for points with a distance of 1.0 m (A), 2.0 m (B), and 3.0 m (C) from the window to examine the trend according to the indoor location. The height of all points is 0.6 m, which is the height of the occupant's sitting position [15]. Figure 7 is a schematic diagram of the location of the target points.

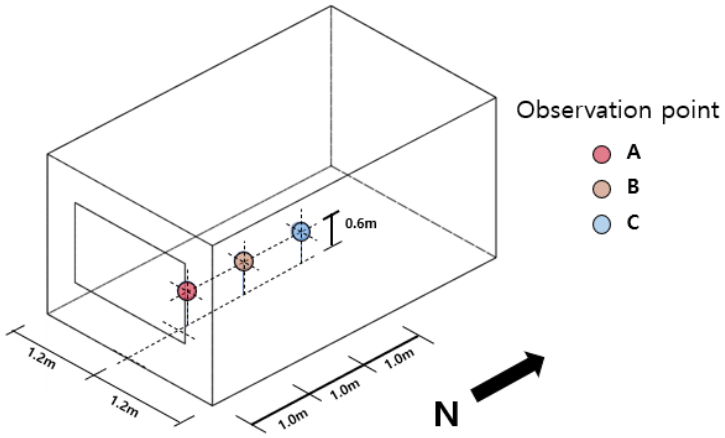


Figure 7. Defined calculation points in the room.

4.1. The Mean Radiant Temperature Algorithm

Mean radiant temperature (MRT) T_r is calculated using the plane radiant temperature presented in the international standard ISO 7726. According to the standard, the MRT is calculated using the plane radiant temperature for each surface and the human body projected area factor for the surface direction, assuming that the occupant is a regular hexahedron. Therefore, the MRT is derived by Equation (1) using the plane radiant temperatures for the six infinitesimal surfaces of the target point.

$$T_r = c_z\left(T_{pr,Top} + T_{pr,Bottom}\right) + c_y\left(T_{pr,Right} + T_{pr,Left}\right) + c_x\left(T_{pr,Front} + T_{pr,Back}\right) \quad (1)$$

where c_z, c_y, c_x are the projected area factors in the z, y, and x directions on the human body surface, and $T_{pr,D}$ is the plane radiation temperature in the D-direction. The projected area factor was entered as the value of the sitting position [15].

For an environment where only long-wave radiation from surrounding surfaces is considered, and other radiation effects are small enough to be negligible, the plane radiation temperature can be calculated as Equation (2) below. However, in a location close to a surface that can transmit solar radiation, such as a window, the plane radiation temperature may rise due to the radiation transmitted into the room. Since Equation (2) does not include solar radiation transmitted into the room, the MRT may be underestimated during the daytime when solar radiation is present. Several results have been reported in the literature that the MRT can be increased by more than 20 °C under the influence of transmitted solar radiation and can cause radiation asymmetry [30].

$$T_{pr,D} = \sqrt[4]{\sum_{i=1}^{N} F_{D\to i} T_{surf,i}^4} \tag{2}$$

where $T_{surf,i}$ means the i-th indoor surface temperature, and $F_{d\to i}$ means the view factor between the D-direction surface of the target point and the surrounding i-th surface.

Since the indoor environment modeled in this study can be affected by irradiance, the plane radiation temperature is calculated by Equation (3) considering the direct and diffuse irradiance transmitted into the room [31].

$$T_{pr,D} = \sqrt[4]{\frac{\alpha_S}{\varepsilon_S}\sum_{i=1}^{N} F_{D\to surf,i} T_{surf,i}^4 + \frac{\alpha_d}{\sigma\varepsilon_S}\sum_{j=1}^{M} F_{D\to surf,j} I_d + C_S \frac{\alpha_b}{\sigma\varepsilon_S} I_b cos\theta_b} \tag{3}$$

where T_{surf} is the surrounding surface temperature, ε_S is the emissivity of the target surface, and σ is the Stefan-Boltzmann constant ($\sigma = 5.67 \times 10^{-8}\ W/m^2K^4$). I_d and α_d indicate the radiation intensity and absorption coefficient of the diffuse solar radiation transmitted into the room. And I_b, α_b, and θ_b mean the radiation intensity, absorption coefficient, and incident angle for the direct solar radiation transmitted into the room, respectively. C_S is a shading coefficient for direct solar radiation.

The absorption coefficient α_s and the emissivity ε_S of the target surface are set to 1 from the black body assumption, but the absorption coefficient α_b and α_d for irradiation can vary depending on the type of clothing worn as well as the skin color of the occupants. These parameters are assumed to be 0.67 for average clothing and skin color (white) [32].

The solar radiation incident through the window can be partially blocked due to the shading effect of the envelope. Therefore, it is necessary to verify whether the target point is affected by the shading effect. This is checked hourly because it changes with the sun's position. The shading effect of the envelope can partially block the solar radiation incident through the window. So it needs to be verified that the target point is affected by the shading effect and this is checked every timestep as it depends on the sun's position.

The area where the direct sunlight Is incident was calculated to confirm the shading effect [33]. This area is determined by the coordinates A, B, C and D points shown in Figure 8. These coordinates can be determined using the su"s position and the geometric parameters of the envelope. (Equations (4)–(11)) When the target point is located within the calculated area, the shading coefficient C_S is 1, otherwise, it is 0.

$$x_A = x_W - \left(\frac{z_W - z_b}{tan\beta} cos\gamma + \frac{s}{2}\right) tan\gamma + \left|\frac{s}{2} tan\gamma\right| \tag{4}$$

$$y_A = \frac{z_W - z_b}{tan\beta} cos\gamma \tag{5}$$

$$x_B = x_W - \left(\frac{H_W + z_W - z_b}{tan\beta} cos\gamma - \frac{s}{2}\right) tan\gamma + \left|\frac{s}{2} tan\gamma\right| \tag{6}$$

$$y_B = \frac{H_W + z_W - z_b}{tan\beta} cos\gamma - s \tag{7}$$

$$x_C = x_W + L_W + \left(\frac{H_W + z_W - z_b}{tan\beta} cos\gamma - \frac{s}{2}\right) tan\gamma - |\frac{s}{2} tan\gamma| \tag{8}$$

$$y_C = \frac{H_W + z_W - z_b}{tan\beta} cos\gamma - s \tag{9}$$

$$x_D = x_W + L_W + \left(\frac{z_W - z_b}{tan\beta} cos\gamma + \frac{s}{2}\right) tan\gamma - |\frac{s}{2} tan\gamma| \tag{10}$$

$$y_D = \frac{z_W - z_b}{tan\beta} cos\gamma \tag{11}$$

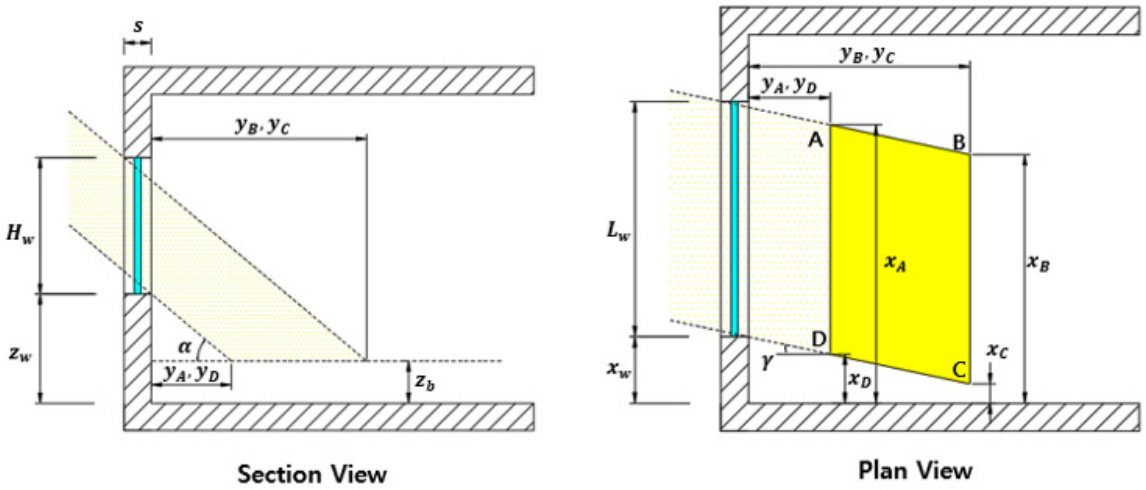


Figure 8. Definition of the geometric parameters involved in the delimitation of the irradiated zone modified with permission from Ref. [33].

The view factor can be calculated by Equation (12). Still, since it is often difficult to apply in actual geometric boundary conditions, the view factor is calculated numerically after being discretized as in Equation (13).

$$F_{d \to j} = \frac{1}{A_i} \iint_{A_i A_d} \frac{cos\theta_i cos\theta_d}{\pi R^2} dA_d dA_i \tag{12}$$

$$F_{d \to j} \approx \frac{1}{A_i} \sum\sum \frac{cos\theta_i cos\theta_d}{\pi R^2} dA_d dA_i \tag{13}$$

where R is the distance between dA_d and dA_i, and θ is the angle between the normal vector of dA_i and the vector connecting the centers of dA_d and dA_i.

4.2. Predicted Mean Vote (PMV)

Predicted Mean Vote (PMV) is used as the thermal comfort index used in this study. PMV represents people's average thermal sensation with the same activity and clothing for a given environment. To comply with ASHRAE 55 [2], the recommended thermal limit on PMV is between −0.5 and 0.5. In the case of ISO 7730 [4], the recommended PMV is between −0.7 and 0.7 for existing buildings, and new buildings range between −0.5 and +0.5. PMV is widely used to evaluate the thermal comfort level of indoor environments such as residential buildings, offices, and hospitals.

According to the procedure presented in ISO-7730 [4], PMV is calculated using 5 physical parameters (i.e., air temperature, relative humidity, air velocity, mean radiant temperature, water vapor pressure) and 2 occupant's parameters (i.e., clo and metabolic

rate). Indoor physical parameters, such as relative humidity, air velocity, and air temperature, are assumed to be uniform throughout the indoor space. The values simulated by EnergyPlus are used.

As shown in Table 3, For the clo value, different values are applied depending on the winter and summer seasons, and the occupant's activity (metabolic rate) is assumed to be a sedentary activity (office, dwelling, school, laboratory). The parameters dependent on the occupant are assumed to be constant during the simulation period.

Table 3. Input parameters for occupant's state.

Parameter Description [Unit]	Winter	Summer
Metabolic rate [W/m^2]	70	70
External work [W/m^2]	0	0
Clo [-]	1.0	0.5

4.3. Uncertainty Analysis Method

In this study, the Monte Carlo method (MCM), a sampling-based method, was used to derive results, including uncertainty. MCM is a widely used uncertainty analysis method in the building energy field, such as GUM (Guide to the expression of uncertainty in measurement), TSM (Taylor Series Method) [34–36]. According to the literature, researchers obtained reliable uncertainty results and objective estimates of mean and variance for thermal comfort using MCM [37,38]. The following process is carried out to derive the MRT uncertainty using MCM.

Considering each clustered surface group G_k as a sample space, one surface is randomly sampled from each group. In this step, all surfaces in the group have the same probability of being sampled. (Equation (14))

$$T_{surf,k} \sim U_k(G_k), G_k = \left\{T_{surf,a}, T_{surf,b}, \ldots.\right\} \tag{14}$$

The temperature of the sampled surface is input to the MRT calculation model f_{MRT}, and the surface is representative of all surfaces in the sampled group. For each sampled surface temperature, 0.5 °C of Gaussian noise is added to reflect the uncertainty of the surface temperature sensor. (Equation (15))

$$T_{r,k} = f_{MRT}(N\left(T_{surf,1}, 0.5\right), \ldots, N\left(T_{surf,k}, 0.5\right)) \tag{15}$$

Therefore, the output is calculated from the MRT model using the temperature sampled on the surface group, as shown in Figure 9. Repeating this process, an MRT sample is collected, and when the number of iterations achieves a set value, an uncertainty indicator is derived from the data generated in all trials.

The uncertainty indicator is expressed as an expanded uncertainty with 95% confidence interval based on the GUM method. When there are sufficient observed samples, and the systematic error is zero, an expanded uncertainty of 95% confidence level $U_{95,k}$ can be obtained by multiplying the standard deviation by two. (Equation (16)) [35] Using MCM, standard deviations are calculated for every time step, and finally these indicators are expressed as expected values for the set simulation period.

$$U_{95,k} = 2\overline{s_k} \tag{16}$$

$$s_k = \sqrt{\frac{\sum_{i=1}^{n}\left(T_{mrt,k} - \overline{T}_{mrt,k}\right)^2}{n}} \tag{17}$$

where k means the number of surfaces used for MRT calculation, and n is the number of MRT data for each time step (n = 100).

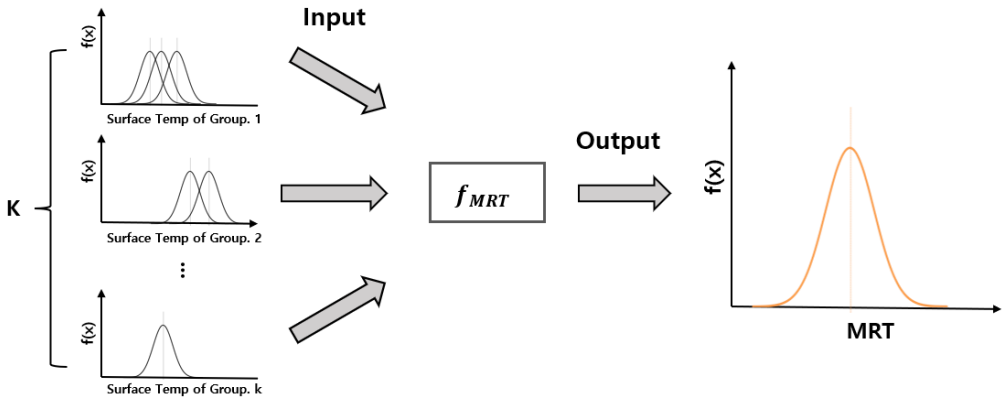


Figure 9. Schematic view of Monte Carlo simulation to estimate the uncertainty of MRT.

5. Results and Discussion

5.1. Uncertainty Analysis of Mean Radiant Temperature

Based on MCM, the uncertainty distribution of MRT was derived. Figure 10 shows a histogram of the MRT uncertainty over the entire simulation period. Except for the MRT calculated with two surfaces, the uncertainty distribution of the other MRTs appeared similar to the normal distribution. The mean and standard deviation of each distribution are shown in Table 4. The uncertainty of the MRT calculated with only two surfaces shows the largest value with an average of about 0.62 °C and a maximum of about 1.1 °C. The uncertainty of MRT calculated with 5 or 6 surfaces is relatively small, with an average of about 0.48 °C and a maximum of 0.59 °C.

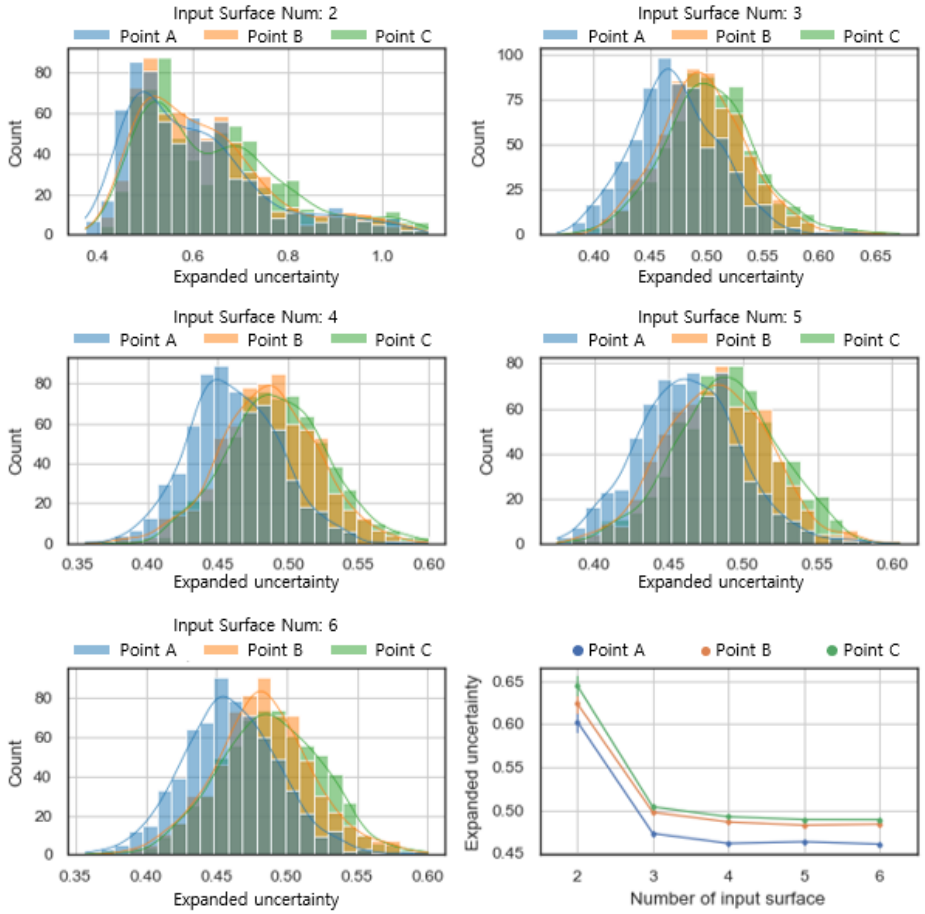


Figure 10. Histogram of expanded uncertainty of MRT calculation results.

Table 4. Summary of the expanded uncertainty of 95% confidence level.

Number of Inputs Surface	Point	Mean	Max	Standard Deviation	Coefficient of Variation
2	A	0.603	1.082	0.144	23.8%
	B	0.623	1.080	0.140	22.4%
	C	0.644	1.097	0.151	23.5%
3	A	0.473	0.627	0.039	8.2%
	B	0.497	0.641	0.039	7.8%
	C	0.504	0.672	0.042	8.3%
4	A	0.461	0.571	0.032	7.0%
	B	0.486	0.600	0.035	7.2%
	C	0.492	0.595	0.035	7.1%
5	A	0.463	0.581	0.034	7.3%
	B	0.483	0.605	0.034	7.1%
	C	0.489	0.586	0.034	7.1%
6	A	0.460	0.587	0.034	7.4%
	B	0.484	0.600	0.035	7.3%
	C	0.489	0.600	0.036	7.4%

The uncertainty tends to decrease as the number of surfaces used in the calculation increases. In particular, when increasing the input surface temperature from 2 to 3, the uncertainty reduction rate was 20% to 22%, showing a great improvement. When the number of input surfaces is increased from 2 to 3, the surfaces facing the outside air (ceiling, south wall) are classified into a new group, and MRT is calculated. In this case, it is judged that individually considering the surfaces facing the outside significantly influences the improvement of the uncertainty.

The uncertainty of $T_{r,4}$ was on average about 2.5% smaller than the uncertainty of $T_{r,3}$. In the case of more than 5 surfaces, the uncertainty change by increasing the input surface was small, within $\pm$1%. The newly added surfaces in $T_{r,5}$ and $T_{r,6}$ are surfaces classified from the surface group facing the adjacent zone. This indicates that the uncertainty change with the addition of the input surface is negligible because the surfaces facing the adjacent zone have similar temperatures.

Comparing the expected uncertainty values at each observation point, the smallest value is shown at point A, which is close to the window, and the largest at point C, which is close to the center of the room. (Figure 10) Uncertainty deviation, according to the observation point, varies from 3% to 10% depending on the number of input surface temperatures. The uncertainty increases as the distance from the window increases. This shows that the uncertainty propagation of the surface temperature can appear variously depending on the target location.

In addition, increasing the distance of the target location from the surfaces considered as individual surfaces (window and south wall) means that the influence of the grouped surfaces increases, which causes additional uncertainty. To investigate the effect of each surface, sensitivity analysis is performed for each surface according to the observation position. For sensitivity analysis, the Sobol method, which can quantitatively express the influence of input variables, is used using SALib, a Python library [39,40]. The Sobol method is a sensitivity analysis method based on variance decomposition. The sensitivity index is defined by dividing the expected value of the variance of the output variable for the input variable by the total variance of the output variable. (Equation (18)).

$$S_i = \frac{E(V(Y|X_{\sim i}))}{V(Y)} \tag{18}$$

where, S is the sensitivity index, X is the input variable, and Y is the model's output.

Figure 11 shows the sensitivity index of each surface to the MRT according to the distance from the south wall. As the distance increases, the sensitivity of the windows and

the south wall decreases, and the sensitivity of other surfaces increases. It means that as the target point gets closer from A to C, the weight of the grouped surface increases so that the MRT uncertainty may increase. The increase was up to 0.1 °C in all cases.

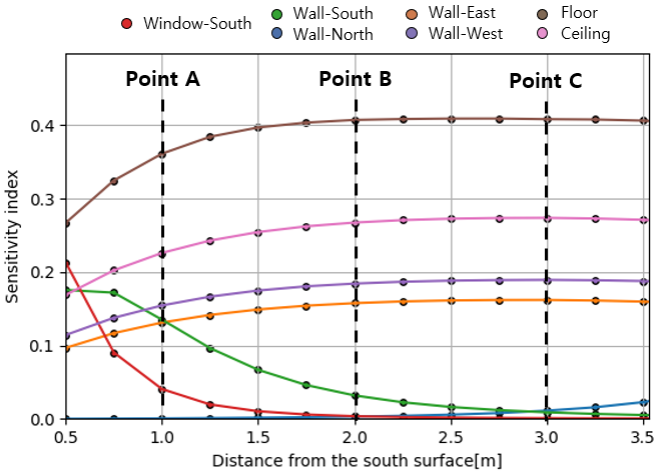


Figure 11. Results of sensitivity analysis.

The uncertainty of MRT according to the number of input surfaces is classified into the winter and summer periods and investigated. Figure 12 shows the expanded uncertainty for winter (left) and summer (right) over 24 h a day. It shows that the time-dependent change of the summer uncertainty and the winter uncertainty is different in $T_{r,2}$. $T_{r,2}$ is MRT calculated with two surface temperatures, and the input surface temperature is randomly selected from a group including only the window surface and a group including all other surfaces.

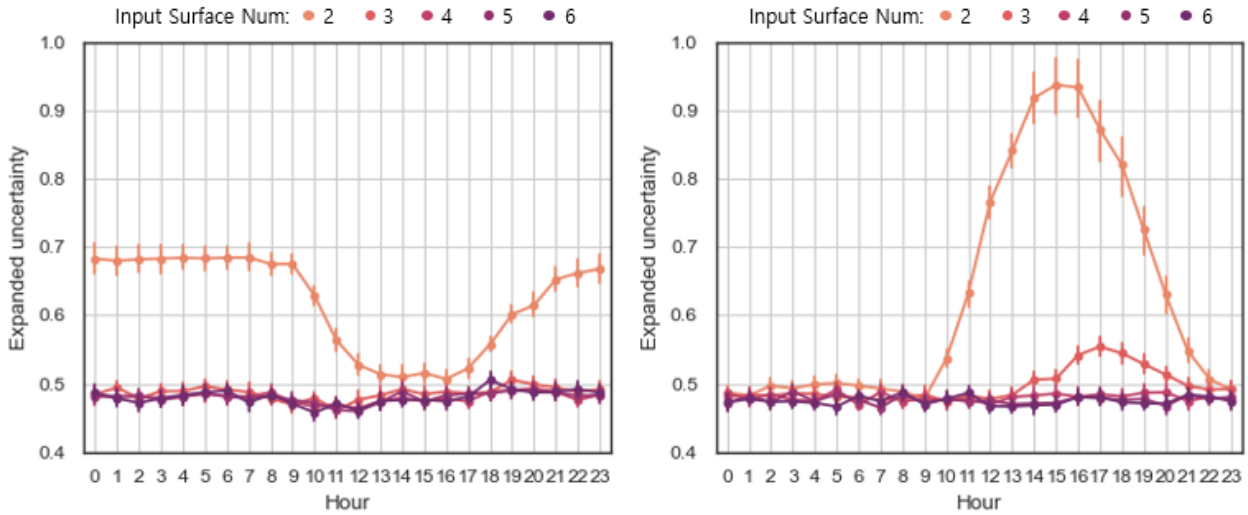


Figure 12. Expanded uncertainty of MRT over 24 h: Winter (**left**), summer (**right**).

In the winter period, the temperature difference between the surfaces in the group increases because the temperature of the surface in contact with the outdoor air is relatively low at night. Therefore, since there are cases where the surface sampled from the group is a surface in contact with the outside air, the MRT may be underestimated, which is a major cause of its uncertainty increase. On the other hand, the uncertainty is higher during the day than at night for the summer period. During the daytime, the temperature difference between the surface in contact with the outside and the rest of the surface increases due to the influence of solar radiation incidents on the envelope. This is a major factor in reducing

the temperature similarity of surfaces within a group and can increase the uncertainty of MRT.

In the case of $T_{r,(k\leq 3)}$, the uncertainty shows a different trend depending on the weather conditions. Figure 13 shows the MRT uncertainty in winter (left) and summer (right) as boxplots according to the number of input surface temperatures. The deviation of the expected value is less than 0.1 °C, showing a slight difference, but the standard deviation of the uncertainty distribution in $T_{r,2}$ is relatively large in summer. The uncertainty of $T_{r,2}$ shows relatively greater fluctuations in summer than in winter. In the case of $T_{r,(k\leq 3)}$, the uncertainty expected value deviation between the two periods is less than 0.1 °C, showing little difference in uncertainty depending on the season.

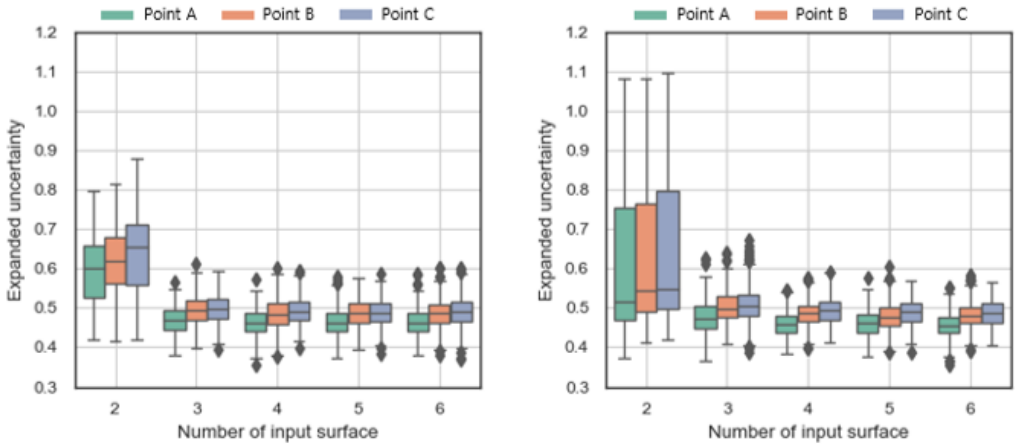


Figure 13. Expanded uncertainty: winter (**left**), summer (**right**).

5.2. Propagation of Uncertainty to Thermal Comfort

The PMV uncertainty is derived using the MRT calculated by the MCM. Figure 14 shows the PMV uncertainty distribution for each season according to the number of input surface temperatures. The uncertainty of PMV shows a similar trend to that of MRT shown in the previous section due to its linear relationship with MRT.

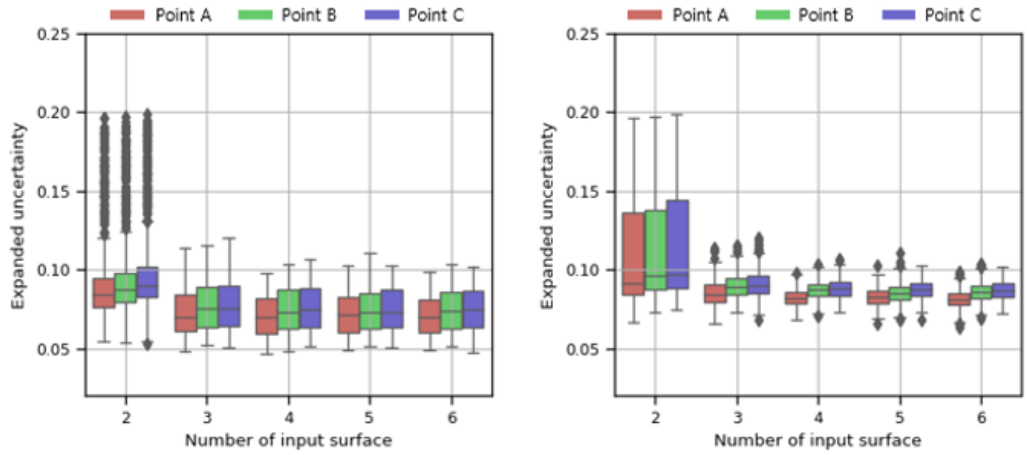


Figure 14. Expanded uncertainty of PMV: winter (**left**), summer (**right**).

As the number of input surfaces increased, the expected value converged to about 0.062 for PMV uncertainty in winter and about 0.084 for PMV uncertainty in summer. In both seasons, the expected value and standard deviation of PMV uncertainty are high at $T_{r,2}$, but the PMV uncertainties calculated from $T_{r,(k>3)}$ show similar values without large deviations. Additionally, the range of expected PMV uncertainty at $T_{r,(k>3)}$ is 0.060–0.088, which are not exceeding 0.1 for most of the observation period.

The uncertainty propagation of PMV shows different characteristics in summer and winter. The expected value of PMV uncertainty was 27–30% higher in summer than in winter. The main reason for the difference was the propagation of uncertainty according to the input clo, since PMV reflects the heat transfer between the occupant and the surrounding environment according to the clo value. As a result, the lower the clo value, the greater the effect of radiation and convection by the surrounding environment, so the uncertainty propagation of MRT becomes relatively large under the condition of wearing light clothing. Figure 15 is a graph showing the uncertainty of PMV propagated by MRT uncertainty by clo value. The PMV distributions are calculated using Monte Carlo simulations for six clothing conditions. It shows that the uncertainty of PMV decreases as the clo value increases.

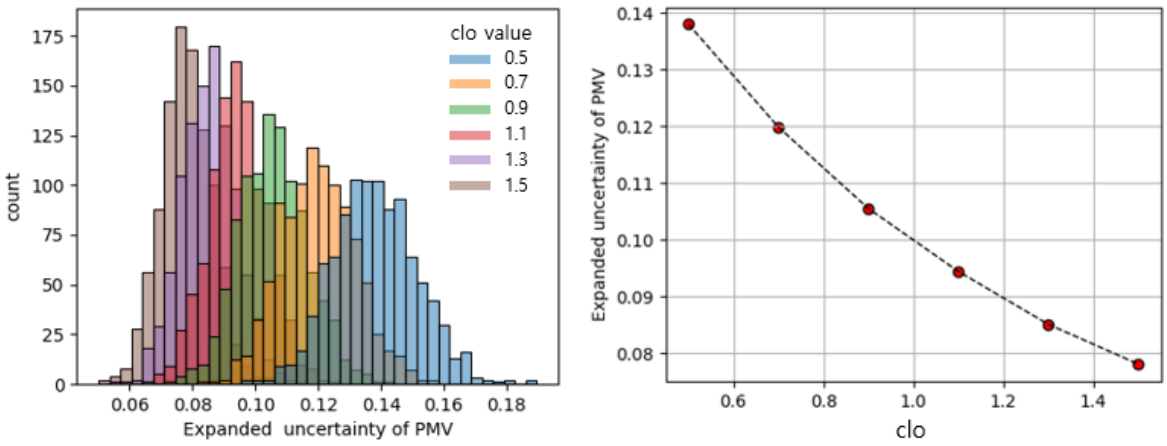


Figure 15. Propagation of uncertainty in PMV by clo value.

6. Conclusions

In this study, MRT was calculated using grouped surface temperatures to investigate the possibility of data monitoring cost savings for MRT observation, and uncertainty due to input surface temperature reduction was analyzed using MCM. The results are summarized as follows:

1. As the number of input surface temperatures used for MRT calculation decreased, the uncertainty increased up to 0.64 °C. This uncertainty change showed a significant difference between $T_{r,2}$ and $T_{r,3}$, and in $T_{r,(k>4)}$, the uncertainty change due to the addition of the input surface was less than 1%. In the case of $T_{r,(k>4)}$, since the surfaces not in contact with the outside show similar temperatures, it was shown that measuring these surfaces individually does not significantly affect the results;
2. When examining the MRT uncertainty according to the observation point, the expected value of the uncertainty increased at the point farther from the southern surface. Since the parameters of the MRT model (view factors for the surrounding surfaces) can vary depending on the observation point, the uncertainty propagated at each surface can also vary. In this case, the uncertainty increased by up to 0.1 °C as the observation point approached the grouped surface;
3. In $T_{r,(k\leq3)}$, when only the surface in contact with the outside was selected, the MRT uncertainty tended to fluctuate according to the weather conditions. For stable MRT observation, it is necessary to appropriately select a surface that can be representative of the other surfaces in the group;
4. As a result of investigating the effect of MRT uncertainty on PMV uncertainty, the expected value of PMV uncertainty was about 30% higher in summer than in winter. This is a result of the input clothing value difference, and the lighter the occupant's clothing, the greater the MRT's effect on PMV.

As the results indicate, it was found that excluding surfaces with similar temperatures for MRT estimation did not significantly affect the uncertainty. Observation of MRT

using only representative surfaces through preliminary research shows the possibility of effectively reducing the cost of data measurement. As to limitations, since this study was conducted under limited indoor conditions, the number of surface temperatures required, and the uncertainty may vary depending on the characteristics of the applied zone. Hence, more geometry and zone types with different indoor conditions should be investigated to validate our results further.

Author Contributions: Conceptualization, D.K.; methodology, H.C.; software, E.K.; validation, R.L.; formal analysis, H.C.; investigation, E.K.; resources J.Y.; data curation, R.L.; writing—original draft preparation, E.K.; writing—review and editing, D.K.; visualization, R.L.; supervision, D.K.; project administration, J.Y.; funding acquisition, J.Y. All authors have read and agreed to the published version of the manuscript.

Funding: This work is supported by the Korea Agency for Infrastructure Technology Advancement (KAIA) grant funded by the Ministry of Land, Infrastructure and Transport (Grant 21CTAP-C163698-01).

Data Availability Statement: The data presented in this study are available on request from the corresponding author.

Acknowledgments: The authors wish to acknowledge supports from the Korea Agency for Infrastructure Technology Advancement (21CTAP-C163698-01).

Conflicts of Interest: The authors declare no conflict of interest.

References

1. Jiang, Y.; Wang, Z.; Lin, B.; Mumovic, D. Development of a Health Data-Driven Model for a Thermal Comfort Study. *Build. Environ.* **2020**, *177*, 106874. [CrossRef]
2. *ASHRAE Standard 55*; Thermal Environmental Conditions for Human Occupancy. The American Society of Heating, Refrigerating and Air-Conditioning Engineers, Inc.: Atlanta, GA, USA, 2013.
3. Fanger, P.O. *Thermal Comfort: Analysis and Applications in Environmental Engineering*; Mcgraw-Hill: New York, NY, USA, 1970.
4. *ISO 7730:2005 Ergonomics of the Thermal Environment—Analytical Determination and Interpretation of Thermal Comfort Using Calculation of the PMV and PPD Indices and Local Thermal Comfort Criteria*, 3rd ed.; International Organization for Standardization: Geneva, Switzerland, 2005.
5. Kim, J.; Schiavon, S.; Brager, G. Personal Comfort Models–A New Paradigm in Thermal Comfort for Occupant-Centric Environmental Control. *Build. Environ.* **2018**, *132*, 114–124. [CrossRef]
6. Fanger, P.O. Local Discomfort to the Human Body Caused by Non-Uniform Thermal Environments. *Ann. Occup. Hyg.* **1977**, *20*, 285–291. [CrossRef] [PubMed]
7. McNall, P.E.; Biddison, R.E. Thermal and Comfort Sensations of Sedentary Persons Exposed to Asymmetric Radiant Fields. *ASHRAE Trans.* **1970**, *76*, 123–136.
8. Özbey, M.F.; Turhan, C. A Comprehensive Comparison and Accuracy of Different Methods to Obtain Mean Radiant Temperature in Indoor Environment. *Therm. Sci. Eng. Prog.* **2022**, *31*, 101295. [CrossRef]
9. Alfano, F.R.D.A.; Dell'Isola, M.; Palella, B.I.; Riccio, G.; Russi, A. On the Measurement of the Mean Radiant Temperature and Its Influence on the Indoor Thermal Environment Assessment. *Build. Environ.* **2013**, *63*, 79–88. [CrossRef]
10. Guo, H.; Ferrara, M.; Coleman, J.; Loyola, M.; Meggers, F. Simulation and Measurement of Air Temperatures and Mean Radiant Temperatures in a Radiantly Heated Indoor Space. *Energy* **2020**, *193*, 116369. [CrossRef]
11. Ekici, C. Measurement Uncertainty Budget of the PMV Thermal Comfort Equation. *Int. J. Thermophys.* **2016**, *37*, 48. [CrossRef]
12. Chaudhuri, T.; Soh, Y.C.; Bose, S.; Xie, L.; Li, H. On Assuming Mean Radiant Temperature Equal to Air Temperature during PMV-Based Thermal Comfort Study in Air-Conditioned Buildings. In Proceedings of the IECON 2016-42nd Annual Conference of the IEEE Industrial Electronics Society, Florence, Italy, 23–26 October 2016; pp. 7065–7070.
13. Halawa, E.; van Hoof, J.; Soebarto, V. The Impacts of the Thermal Radiation Field on Thermal Comfort, Energy Consumption and Control—A Critical Overview. *Renew. Sustain. Energy Rev.* **2014**, *37*, 907–918. [CrossRef]
14. Wang, D.; Chen, G.; Song, C.; Liu, Y.; He, W.; Zeng, T.; Liu, J. Experimental Study on Coupling Effect of Indoor Air Temperature and Radiant Temperature on Human Thermal Comfort in Non-Uniform Thermal Environment. *Build. Environ.* **2019**, *165*, 106387. [CrossRef]
15. Atmaca, İ.; Kaynaklı, Ö.; Yiğit, A. Effects of Radiant Temperature on Thermal Comfort. *Build. Environ.* **2007**, *42*, 3210–3220. [CrossRef]
16. *Standard ISO 7726*; Ergonomics of the Thermal Environment-Instruments for Measuring Physical Quantities. International Organization for Standardization: Geneva, Switzerland, 1998.
17. Da Silva, M.G.; Santana, M.M.; e Sousa, J.A. Uncertainty Analysis of the Mean Radiant Temperature Measurement Based on Globe Temperature Probes. *J. Phys. Conf. Ser.* **2018**, *1065*, 072036. [CrossRef]

18. Lee, D.-S.; Kim, E.-J.; Cho, Y.-H.; Kang, J.-W.; Jo, J.-H. A Field Study on Application of Infrared Thermography for Estimating Mean Radiant Temperatures in Large Stadiums. *Energy Build.* **2019**, *202*, 109360. [CrossRef]
19. ISO. *ISO 9869-2: 2018—Thermal Insulation—Building Elements—In-Situ Measurement of Thermal Resistance and Thermal Transmittance—Part 2: Infrared* Method for Frame Structure Dwelling; International Organization for Standardization: Geneva, Switzerland, 2018.
20. Vorre, M.H.; Jensen, R.L.; le Dréau, J. Radiation Exchange between Persons and Surfaces for Building Energy Simulations. *Energy Build.* **2015**, *101*, 110–121. [CrossRef]
21. Dogan, T.; Kastner, P.; Mermelstein, R. Surfer: A Fast Simulation Algorithm to Predict Surface Temperatures and Mean Radiant Temperatures in Large Urban Models. *Build. Environ.* **2021**, *196*, 107762. [CrossRef]
22. Alfano, F.R.D.A.; Palella, B.I.; Riccio, G. The Role of Measurement Accuracy on the Thermal Environment Assessment by Means of PMV Index. *Build. Environ.* **2011**, *46*, 1361–1369. [CrossRef]
23. Moutela, R.; Carrilho, J.D.; da Silva, M.G. Sensitivity of the PMV Index to the Thermal Comfort Parameters. In Proceedings of the 2nd Energy for Sustainability Multidisciplinary Conference, Coimbra, Portugal, 14–15 May 2015.
24. Crawley, D.B.; Lawrie, L.K.; Pedersen, C.O.; Winkelmann, F.C. Energy plus: Energy Simulation Program. *ASHRAE J.* **2000**, *42*, 49–56.
25. Loutzenhiser, P.G.; Manz, H.; Felsmann, C.; Strachan, P.A.; Frank, T.H.; Maxwell, G.M. Empirical Validation of Models to Compute Solar Irradiance on Inclined Surfaces for Building Energy Simulation. *Sol. Energy* **2007**, *81*, 254–267. [CrossRef]
26. Chong, A.; Menberg, K. Guidelines for the Bayesian Calibration of Building Energy Models. *Energy Build.* **2018**, *174*, 527–547. [CrossRef]
27. IWEC2 Weather Files. Available online: https://www.Ashrae.Org/Technical-Resources/Bookstore/Ashrae-International-Weather-Files-for-Energy-Calculations-2-0-Iwec2 (accessed on 10 January 2023).
28. McQueen, J.B. Some Methods of Classification and Analysis of Multivariate Observations. In Proceedings of the 5th Berkeley Symposium on Mathematical Statistics and Probability, Berkeley, CA, USA, 21 June–18 July 1965 and 27 December 1965–7 January 1966; pp. 281–297.
29. Pedregosa, F.; Varoquaux, G.; Gramfort, A.; Michel, V.; Thirion, B.; Grisel, O.; Blondel, M.; Prettenhofer, P.; Weiss, R.; Dubourg, V. Scikit-Learn: Machine Learning in Python. *J. Mach. Learn. Res.* **2011**, *12*, 2825–2830.
30. Marino, C.; Nucara, A.; Pietrafesa, M. Thermal Comfort in Indoor Environment: Effect of the Solar Radiation on the Radiant Temperature Asymmetry. *Sol. Energy* **2017**, *144*, 295–309. [CrossRef]
31. La Gennusa, M.; Nucara, A.; Rizzo, G.; Scaccianoce, G. The Calculation of the Mean Radiant Temperature of a Subject Exposed to the Solar Radiation—A Generalised Algorithm. *Build. Environ.* **2005**, *40*, 367–375. [CrossRef]
32. Blum, H.F. The Solar Heat Load: Its Relationship to Total Heat Load and Its Relative Importance in the Design of Clothing. *J. Clin. Investig.* **1945**, *24*, 712–721. [CrossRef] [PubMed]
33. La Gennusa, M.; Nucara, A.; Pietrafesa, M.; Rizzo, G. A Model for Managing and Evaluating Solar Radiation for Indoor Thermal Comfort. *Sol. Energy* **2007**, *81*, 594–606. [CrossRef]
34. Joint Committee for Guides in Metrology (JCGM), Supplement 1 to the 'Guide to the Expression of Uncertainty in Measurement'—Propagation of Distributions Using a Monte Carlo Method JCGM 101:2008. 2008. Available online: http://www.bipm.org/utils/common/documents/jcgm/JCGM_100_2008_E.pdf (accessed on 10 January 2023).
35. Tian, W.; Heo, Y.; de Wilde, P.; Li, Z.; Yan, D.; Park, C.S.; Feng, X.; Augenbroe, G. A Review of Uncertainty Analysis in Building Energy Assessment. *Renew. Sustain. Energy Rev.* **2018**, *93*, 285–301. [CrossRef]
36. Cho, H.; Smith, A.; Luck, R.; Mago, P.J. Transient Uncertainty Analysis in Solar Thermal System Modeling. *J. Uncertain. Anal. Appl.* **2017**, *5*, 1–15. [CrossRef]
37. Broday, E.E.; Ruivo, C.R.; da Silva, M.G. The Use of Monte Carlo Method to Assess the Uncertainty of Thermal Comfort Indices PMV and PPD: Benefits of Using a Measuring Set with an Operative Temperature Probe. *J. Build. Eng.* **2021**, *35*, 101961. [CrossRef]
38. Ricciu, R.; Galatioto, A.; Desogus, G.; Besalduch, L.A. Uncertainty in the Evaluation of the Predicted Mean Vote Index Using Monte Carlo Analysis. *J. Environ. Manag.* **2018**, *223*, 16–22. [CrossRef] [PubMed]
39. Herman, J.; Usher, W. SALib: An Open-Source Python Library for Sensitivity Analysis. *J. Open Source Softw.* **2017**, *2*, 97. [CrossRef]
40. Saltelli, A.; Annoni, P.; Azzini, I.; Campolongo, F.; Ratto, M.; Tarantola, S. Variance Based Sensitivity Analysis of Model Output. Design and Estimator for the Total Sensitivity Index. *Comput. Phys. Commun.* **2010**, *181*, 259–270. [CrossRef]

Disclaimer/Publisher's Note: The statements, opinions and data contained in all publications are solely those of the individual author(s) and contributor(s) and not of MDPI and/or the editor(s). MDPI and/or the editor(s) disclaim responsibility for any injury to people or property resulting from any ideas, methods, instructions or products referred to in the content.